## A GENERIC GROUND DYNAMICS MODEL FOR GROUND HANDLING EVALUATIONS

**Göktuğ Koçak**
goktug.kocak@tai.com.tr
Design Engineer

**Kaan Şansal**
kaan.sansal@tai.com.tr
Design Engineer

**Serkan Sağıroğlu**
ssagiroglu@tai.com.tr
Technical Specialist

**Volkan Kargın**
vkargin@tai.com.tr
Senior Technical Specialist

Turkish Aerospace Industries Inc.
Ankara, Turkey

### ABSTRACT

This paper demonstrates a generic ground dynamics model for modeling and simulating landing gear systems. Physics based model is developed in MATLAB-Simulink® environment and it is integrated to a non-linear 6-DOF helicopter model which is constructed in an in-house comprehensive analysis code, TAI Originated Rotorcraft Simulation (TOROS). Other than simulating the helicopter motion after touchdown, this model is also capable of trimming the helicopter on ground, which is useful for determining landing and take-off capabilities of a helicopter on either a flat or a sloped surface. This method can show whether the control ranges are adequate or not during the design stage, which is a troublesome task during preliminary design. In this study, slope-landing analyses of a light utility helicopter is demonstrated together with dynamics of a generic landing gear. The effect of ground on non-uniform inflow parameters, which is capable of modelling inclined ground effect, is included into the non-linear mathematical model using a finite state approach. Results show that, finite state ground effect model affected the control margins and main rotor flapping during slope landing and take-off analyses. In addition, rotational degree of freedom is added to the wheel component, which can be utilized not only for trimming and linearizing the helicopter on ground with/without airspeed but also for performing different ground-handling evaluations (e.g. high-speed taxiing, rolling take-off etc.). Moreover, by using this mathematical model, spin-up loads during run-on landings can be calculated, landing distance to full stop can be found and failure simulations (e.g. flat tire) can be performed.

### 1 NOTATION

| | |
|---|---|
| $C_{bg}$ | Ground to body transformation matrix |
| $C_{int_{fr}}$ | Internal friction coefficient, kg/s |
| $c_{t_x}$ | Tire longitudinal damping, kg/s |
| $c_{t_y}$ | Tire lateral damping, kg/s |
| $F_b$ | Forces transmitted to helicopter body, N |
| $F_{damp}$ | Strut damping force, N |
| $F_{f_x}$ | Longitudinal friction force, N |
| $F_{f_y}$ | Lateral friction force, N |
| $f_k$ | Kinetic friction coefficient, nd |
| $f_s$ | Static friction coefficient, nd |
| $F_{sp}$ | Strut spring force, N |
| $F_{st}$ | Total strut force, N |
| $F_{tb}$ | Tire forces in body axis, N |
| $F_{y_{coeff1,2}}$ | 1st and 2nd dynamic friction coefficients, nd |
| $[G]$ | Ground influence coefficients matrix |
| $h$ | Tire distance from ground, m |
| $k_{rim}$ | Rim stiffness, kg/s$^2$ |
| $k_{surf}$ | Ground surface quality factor, nd |
| $k_{t_x}$ | Tire longitudinal stiffness, kg/s$^2$ |
| $k_{t_y}$ | Tire lateral stiffness, kg/s$^2$ |
| $k_{t_z}$ | Tire vertical stiffness, kg/s$^2$ |
| $[L]$ | Induced inflow gain matrix |
| $[M]$ | Apparent mass matrix |
| $M_b$ | Moments transmitted to H/C body, Nm |
| $M_{int_{fr}}$ | Internal friction torque at the wheel axle |
| $N_t$ | Tire normal force, N |
| $p_b, q_b, r_b$ | Body Angular rates, rad/s |
| $R_w$ | Radius of wheel, m |
| $S_x$ | Slip Ratio, nd |
| $T_{br}$ | Brake Torque |
| $V_m$ | Mass flow parameter |
| $V_{slip}$ | Slip Velocity, m/s |
| $V_{tb}$ | Tire velocity in body axis, m/s |
| $V_{tg}$ | Tire velocity in ground axis, m/s |
| $w$ | Induced velocity |
| $x_{rad}$ | Radial distance between tire contact patch and wheel axle, m |
| $x_t, y_t, z_t$ | Position of tires w.r.t. helicopter c.g., m |
| $\alpha_j^r$ | Rotor induced inflow coeffs. in terms of $\phi_j^r$ |
| $\beta$ | Decay factor of friction, nd |
| $\beta_s$ | Tire skid angle, rad |
| $\gamma_N, \gamma_E$ | North and east ground slope angles, rad |
| $\delta$ | Ground declination angle, deg |
| $\delta_{brake}$ | Brake pedal input, nd |
| $\delta_{st}$ | Strut deflection, m |
| $\dot{\delta}_{st}$ | Strut velocity, m/s |
| $\ddot{\delta}_{st}$ | Strut acceleration, m/s$^2$ |
| $\delta_{t_x}$ | Tire longitudinal deflection, m |
| $\delta_{t_y}$ | Tire lateral deflection, m |
| $\delta_{t_z}$ | Tire vertical deflection, m |
| $\dot{\delta}_{t_x}$ | Tire longitudinal velocity, m/s |

Presented at 44th European Rotorcraft Forum, Delft, The Netherlands, 19-20 September, 2018. 

| | |
|---|---|
| $\dot{\delta}_{t_y}$ | Tire lateral velocity, m/s |
| $\mu_{brake}$ | Brake friction coefficient, nd |
| $\mu_{roll}$ | Rolling friction coefficient, nd |
| $\mu_{TireSta}$ | Tire degradation factor, nd |
| $\mu_x$ | Longitudinal friction coefficient, nd |
| $\mu_y$ | Lateral friction coefficient, nd |
| $\tau$ | Rotor pressure potential coefficient |
| $\phi, \theta, \psi$ | Euler angles, rad |
| $\phi_j^r$ | Radial expansion shape function of inflow |
| $\Omega_w$ | Angular speed of wheel axle, rad/s |
| $\dot{\Omega}_w$ | Angular acceleration of wheel axle, rad/s$^2$ |

*Subscripts*

| | |
|---|---|
| $(\ )_b$ | Body-axes frame of reference |
| $(\ )_g$ | Ground-axes frame of reference |
| $(\ )_n, (\ )_j$ | Associated with n$^{th}$, j$^{th}$ radial mode shape |

*Superscripts*

| | |
|---|---|
| $(\ )^c, (\ )^s$ | Cosine, sine part |
| $(\ )^{IGE}$ | In ground effect |
| $(\ )^m$ | Highest azimuthal harmonics |
| $(\ )^r$ | Highest radial harmonics |

## 2 INTRODUCTION

As two of the most dangerous flight phases are take-off and landing, modeling and simulation of a landing gear subsystem becomes an important task. Developing mathematical models using computational design tools lessen both time and cost required during design process.

In literature, various landing gear models with high complexity levels exist. For instance, Daniels [1] includes nonlinear effects to his model such as polytrophic gas law, velocity squared damping and stick-slip friction effects. McGehee et al. [2], include first-mode wing bending and torsional characteristics, oleo pneumatic shock strut with fit and binding friction and empirical tire force-deflection characteristics. These detailed models are useful for design and analysis but they are computationally intensive. For trim and real-time simulations, simplified models can be used as proposed in [3]. In simplified landing gear models, gear reaction forces and moments imparted to the aircraft are calculated by treating strut and tire as simplified spring, mass, damper systems [4].

Other than using a landing gear model as a design and validation tool, a generic ground dynamics model, which is coupled with a high fidelity helicopter model, can give accurate estimations of helicopter behavior on ground before conducting any flight test. This model can be used for slope landing and take-off analyses as well as taxi, rolling take-off, run-on landing analyses and spin-up load estimations. As presented in the following sections as well, starting from a quasi-steady hover condition, the helicopter can be trimmed while the uphill tire is in contact with the ground. Slowly changing the body roll/pitch angle until all landing gears are in contact with the ground gives the required pilot controls during the maneuver. Same methodology can be used in piloted evaluation of the handling quality level of the helicopter according to the slope landing requirements defined in [5], as well.

In [6], it is shown that finite-state ground effect model can capture the correct quantitative effect of the ground inclination angle on the induced power of the rotor. In addition, by using the same ground effect model in [6], Iboshi et al. [7] demonstrated blade-flapping motion of a rotor hovering above an inclined plane. However, to our knowledge, this ground effect model has not been coupled with a high fidelity landing gear model for control margin estimation during slope landing/take-off maneuver so far.

In this study, fidelity of the non-linear mathematical model proposed in [8] is increased by adding the effect of ground on non-uniform inflow parameters using a finite state approach, which is capable of modelling inclined ground effect. In addition, rotational degree of freedom is added to the wheel component, which enables different ground handling evaluations to be performed.

In the first section of the paper, comprehensive analysis tool used for modelling high fidelity non-linear mathematical model of the helicopter will be presented. Next, landing gear dynamics will be described in detail. In the third section, finite state ground effect model on full and inclined surfaces will be discussed. This section will be followed by trim analyses and simulation results.

## 3 HELICOPTER MODEL

TAI Originated Rotorcraft Simulation (TOROS) is an in-house rotorcraft simulation tool built in MATLAB-Simulink® environment. It is used to support flight mechanics design and analysis, handling quality analysis, automatic flight control system design and real-time flight simulation. Each rotorcraft component is modelled individually in a modular structure [8]. Contributions of each component to the equations of motion are calculated based on detailed rotorcraft characteristics. Complexity level of the model developed in TOROS allows it to be used for detailed prediction of whole flight envelope during the design phase.

High fidelity rotorcraft model is constructed by using both FLIGHTLAB® and TOROS. Commercially available software package FLIGHTLAB® is used to validate non-linear mathematical model developed in TOROS in terms of trim, linearized system and non-linear response results [9].

## 4 LANDING GEAR MODEL

In this section, equations of motion of the nonlinear landing gear model used in the study are presented.

Inputs of the non-linear landing gear model are body translational and angular velocities, Euler angles, landing gear coordinates with respect to aircraft cg, height of each tire from the ground and brake percentage applied. Outputs of the model are the forces and moments transferred to the helicopter body. Figure 1 depicts airplane body fixed axis $X_b\ Y_b\ Z_b$ (axis of body & struts), ground fixed axis system $X_g\ Y_g\ Z_g$ (axis of ground & tires) and inertial axis XYZ.

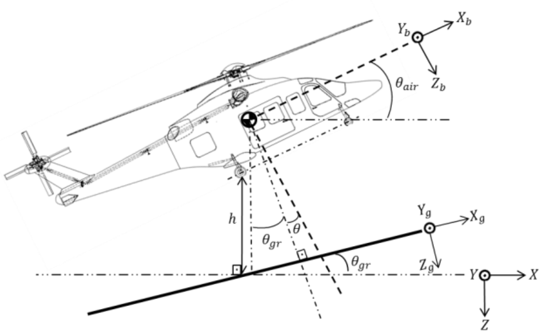


**Figure 1 Coordinate Systems**

Describing positive north and east slope angles as in Figure 2, ground slope angles are transformed into body axis by rotating them about Z axis over an angle $\psi_{air}$ which is called the heading angle;

(1) $\phi_{gr} = \sin(\psi_{air})\,\gamma_N - \cos(\psi_{air})\,\gamma_E$

(2) $\theta_{gr} = \cos(\psi_{air})\,\gamma_N + \sin(\psi_{air})\,\gamma_E$

Ground slope angles are then subtracted from roll and pitch angles of the helicopter body to find the roll ($\phi$) and pitch ($\theta$) angles including the ground slope.

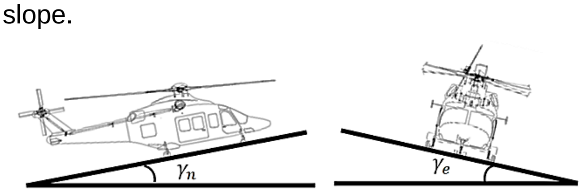


**Figure 2 Positive north and east ground slopes**

For tire contact with ground plane, ground altitude of each tire is checked. Deflection of each tire in vertical axis can be calculated as in (3).

(3) $\delta_{t_z} = h\cos(\phi_{gr})\cos(\theta_{gr}) - \delta_{st}\cos(\phi)\cos(\theta)$

where $\delta_{st}$ term represents strut deflection.

Body axes are rotated in the sequence; ψ about Z, θ about Y and ϕ about X to reach the ground axes system.

(4) $C_{bg} = \begin{bmatrix} \cos\theta & 0 & -\sin\theta \\ \sin\theta\sin\phi & \cos\phi & \cos\theta\sin\phi \\ \sin\theta\cos\phi & -\sin\phi & \cos\theta\cos\phi \end{bmatrix}$

As tires deflect under force, their position with respect to aircraft cg changes. Taking this change into consideration, velocity of each tire in ground axis can be calculated as

(5) $\begin{bmatrix} u_{tg} \\ v_{tg} \\ w_{tg} \end{bmatrix} = C_{bg}^T \begin{bmatrix} u_{tb} \\ v_{tb} \\ w_{tb} \end{bmatrix} + \left[C_{bg}^T \omega_b\right] x \begin{bmatrix} \delta_{t_x} \\ \delta_{t_y} \\ \delta_{t_z} \end{bmatrix}$

Where $\delta_{t_x}$ and $\delta_{t_y}$ represent tire longitudinal and lateral deflections respectively.

(6) $u_{tb} = u_b + q_b z_t - r_b y_t$

(7) $v_{tb} = v_b + r_b x_t - p_b z_t$

(8) $w_{tb} = (w_b - \dot{\delta}_{st}) + p_b y_t - q_b x_t$

Gear forces are computed using non-linear strut deflection vs. force and strut velocity vs. force tables. For the calculation of damping force, other than strut velocity, strut deflection is required. Notice that, total gear forces are found simply by adding these two forces.

(9) $F_{st} = -F_{sp}(\delta_{st}) - F_{damp}(\dot{\delta}_{st}, \delta_{st})$

In the landing gear model, tire degradation factor is included. This factor is multiplied with tire vertical stiffness to represent the effect of different tire pressures. In real life, excessive air in the tire would raise the spring coefficient and lacking air pressure lowers the spring coefficient until the point the spring coefficient becomes zero where tire blows out [10].This feature enables landing and taxi simulations under abnormal conditions.

(10) $k_{t_z} = \mu_{TireSta} \cdot k_{t_z}$

Notice that if ( $\mu_{TireSta} = 0$), tire is blown. Moreover, if the tire saturates, then rim is touching the ground and tire stiffness is modified accordingly.

Normal force due to ground contact, which is the source of friction forces in lateral and longitudinal directions, can be calculated as

(11) $$N_t = \begin{cases} -k_{t_z}\delta_{t_z} & \text{for } \delta_{t_z} < \delta_{t_{z_{max}}} \\ -k_{t_z}\delta_{t_z} + k_{rim}\left(\delta_{t_z} - \delta_{t_{z_{max}}}\right) & \text{for } \delta_{t_z} \geq \delta_{t_{z_{max}}} \end{cases}$$

If rim is touching the ground, rolling friction coefficient is forced to its maximum value, $\mu_{roll} = \mu_{roll_{max}}$.

By knowing the normal force of the tire, maximum frictional forces in both longitudinal ($X_g$) and lateral ($Y_g$) directions can be found. In case of frictional forces along longitudinal direction, the effect of braking force is included. Maximum friction force is applied when the tire is moving along that direction.

For longitudinal friction forces, brake coefficient of friction ($\mu_{brake}$) can be modelled as a function of tire velocity in $X_g$ axis( $u_{tg}$). Different brake coefficients can be used for dry, wet and icy surfaces. Nominal kinetic friction coefficient is calculated as

(12) $$f_{k_{nom}} = \mu_{roll} + (\mu_{brake} - \mu_{roll})\delta_{brake}$$

$\mu_{roll}$ can either be a constant or a function of total velocity in ground axis $V_{tg} = \sqrt{u_{tg}^2 + v_{tg}^2}$.

$f_{k_{x_{nom}}}$ coefficient is modified depending on tire status, which enables maximum friction force to be applied when tire is blown.

(13) $$f_{k_x} = f_{k_{x_{nom}}} + \left(\mu_{brake} - f_{k_{x_{nom}}}\right)(1 - \mu_{TireSta})$$

When there is wheel (i.e. rolling degree of freedom), longitudinal friction coefficient depends on slip ratio which can be calculated as;

(14) $$S_x = \min\left[\frac{|V_{slip}|}{max\left(|u_{tg}|, 0.001\right)}, 1\right]$$

Where $V_{slip} = u_{tg} - \Omega_w x_{rad}$ is the slip velocity and $x_{rad}$ is the radial distance between tire contact patch and wheel axle, which can be obtained as

(15) $$x_{rad} = R_w - \delta_{t_z}$$

If tire is rolling freely, $S_x$ = 0 and if tire is sliding without rotation, $S_x$ = 1.

Figure 3 shows variation of $f_{k_{x_{slip}}}$ with respect to slip ratio. Notice that when slip ratio is between 0.15-0.25 maximum amount of friction is applied to the rotorcraft.

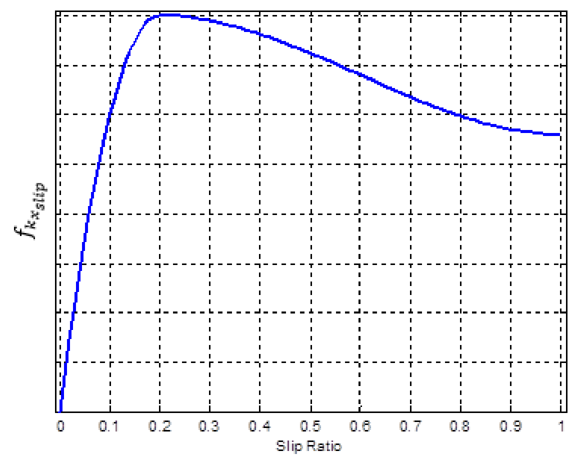


**Figure 3 Longitudinal Friction Coefficient vs. Slip Ratio**

Applying static to kinetic transition, longitudinal friction coefficient can be calculated as

(16) $$\mu_x = k_{surf}\left(f_{k_{x_{slip}}} + \left(f_{k_x} - f_{k_{x_{slip}}}\right)e^{-\beta|V_{slip}|}\right)$$

$\beta$ term given in (16) is called the decay factor of friction and $k_{surf}$ term is called ground surface quality factor and it is used to alter surface quality. Summing up all these effects, maximum friction force in longitudinal direction is found as

(17) $$F_{fx_{max}} = \mu_x|N_t|$$

For kinetic friction coefficient in lateral direction, the effect of skid angle is included which is given in (18).

(18) $$f_{k_{nom}} = F_{y_{coeff1}} \tanh\left(\frac{\left|\frac{\beta_s}{N_t}\right|}{F_{y_{coeff2}}}\right)$$

The skid angle of tires is taken as 0º if the corresponding wheel is caster. If the wheel is not caster, it is taken as

(19) $$\beta_s = atan2(v_{tg}, u_{tg})$$

Including tire status;

(20) $$f_{k_y} = f_{k_{y_{nom}}} + \left(F_{y_{coeff1}} - f_{k_{y_{nom}}}\right)(1 - \mu_{TireSta})$$

(21) $$\mu_y = k_{surf}\left(f_{k_y} + \left(f_{s_y} - f_{k_y}\right)e^{-\beta|V_{tg}|}\right)$$

Summing up all these effects, maximum friction force in lateral direction can found as

(22) $$F_{fy_{max}} = \mu_y|N_t|$$

Tire is modelled as a spring-damper system in both longitudinal and lateral directions as shown in Figure 4, which enables trimming and stopping helicopter on ground.

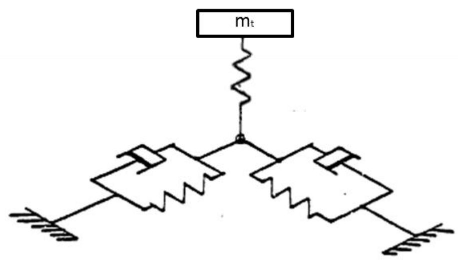


**Figure 4 Tire representation** [4]

Deflections of tire in both directions are calculated by integrating the change of deflections in each axis. Tire forces exerted in longitudinal and lateral axes can then be calculated as

$$(23) \quad F_{sp_{t_x}} = -k_{x_t}\delta_{t_x} - c_{x_t}\dot{\delta}_{t_x}$$

$$(24) \quad F_{sp_{t_y}} = -k_{y_t}\delta_{t_y} - c_{y_t}\dot{\delta}_{t_y}$$

Where $\dot{\delta}_{t_x}$ and $\dot{\delta}_{t_y}$ terms are simply $V_{slip}$ and $v_{tg}$ respectively.

Friction forces acting on helicopter body are limited by maximum friction forces along that direction.

$$(25) \quad F_{fx} = max\left(min\left(F_{sp_{t_x}}, F_{f_{x_{max}}}\right), -F_{f_{x_{max}}}\right)$$

$$(26) \quad F_{fy} = max\left(min\left(F_{sp_{t_y}}, F_{f_{y_{max}}}\right), -F_{f_{y_{max}}}\right)$$

When rolling degree of freedom of wheels is included, tire rolling acceleration can be computed as follows

$$(27) \quad \dot{\Omega}_w = \frac{F_{fx}x_{rad} + N_t\delta_{t_x} - M_{int_{fr}} + T_{br}}{I_w}$$

Where $M_{int_{fr}}$ and $T_{br}$ terms represent internal friction torque at the wheel axle and brake torque respectively. $M_{int_{fr}}$ can be modelled as a function of tire rotation speed

$$(28) \quad M_{int_{fr}} = C_{int_{fr}}\Omega_w$$

Whereas brake torque can be calculated as

$$(29) \quad T_{br} = -K_{br}\theta_{br} - C_{br}\Omega_{br}$$

$\Omega_{br}$ term given in (29) is equal to $\Omega_w$, and the brake deflection, $\theta_{br}$ can be obtained simply by integrating $\Omega_{br}$.

Brake torque is limited with amount of brake applied and maximum brake torque that the braking system allows.

$$(30) \quad T_{br_{lim}} = \delta_{brake}T_{br_{max}}$$

If $|T_{br}| > T_{br_{lim}}$, $\Omega_{br}$ is forced to zero to prevent integrator wind-up and maximum amount of brake torque is applied to the disc.

After computing all forces acting on tires, forces and moments acting on tires in body axis can be found as

$$(31) \quad F_{tb} = \begin{Bmatrix} F_{xtb} \\ F_{ytb} \\ F_{ztb} \end{Bmatrix} = C_{bg}\begin{Bmatrix} F_{fx} \\ F_{fy} \\ N_t \end{Bmatrix}$$

$$(32) \quad M_{tb} = \begin{Bmatrix} M_{xtb} \\ M_{ytb} \\ M_{ztb} \end{Bmatrix} = C_{bg}\left(\begin{Bmatrix} \delta_{t_x} \\ \delta_{t_y} \\ \delta_{t_z} \end{Bmatrix} x \begin{Bmatrix} F_{fx} \\ F_{fy} \\ N_t \end{Bmatrix}\right)$$

Deflections and velocities of the struts are then calculated and fed back to the model by simply integrating their accelerations

$$(33) \quad \ddot{\delta}_{st} = \frac{(F_{st} - F_{ztb})}{m_t}$$

In simulation, if maximum strut deflection is reached, struts behave like a rigid body and tire forces are transferred to the body directly. In that case;

$$(34) \quad F_b = \begin{Bmatrix} F_{xb} \\ F_{yb} \\ F_{zb} \end{Bmatrix} = F_{tb} = \begin{Bmatrix} F_{xtb} \\ F_{ytb} \\ F_{ztb} \end{Bmatrix}$$

$$(35) \quad \ddot{\delta}_{st} = 0$$

In all other cases (when strut limits are not reached or when performing ground trim) forces transferred to helicopter body are

$$(36) \quad F_b = \begin{Bmatrix} F_{xb} \\ F_{yb} \\ F_{zb} \end{Bmatrix} = \begin{Bmatrix} F_{xtb} \\ F_{ytb} \\ F_{st} \end{Bmatrix}$$

Moments transferred to the helicopter body can be calculated as

$$(37) \quad M_b = \begin{Bmatrix} M_{xb} \\ M_{yb} \\ M_{zb} \end{Bmatrix} = r_t \times F_b$$

## 5 FINITE STATE GROUND EFFECT MODEL ON FULL AND INCLINED SURFACES

The finite-state ground effect model used in this study is based on the theory given in Ref. [6]. It is an extension model of the generalized dynamic wake theory [11], which is a three-dimensional and dynamic induced velocity model based on incompressible potential flow assumption. Radial and azimuthal distribution of the induced velocity is expressed by Legendre polynomials and Fourier series expansion respectively as given in (38). It has finite number of states in time domain and is represented in closed form in state-space as first order differential equations given by (39) and (40) for induced flow at rotor disk.

$$w = \sum_r \sum_j \phi_j^r \left[\alpha_j^{rc}(t)\cos(r\psi) + \alpha_j^{rs}(t)\sin(r\psi)\right] \tag{38}$$

$$[M]\{\dot{\alpha}\} + V_m[L]^{-1}\{\alpha\} = \frac{1}{2}\{\tau\} \tag{39}$$

$$\{\alpha\} = \frac{1}{V_m}[L]\left\{\frac{\tau}{2}\right\} \tag{40}$$

$$\{\alpha_j^r\}^{IGE} = \frac{1}{V_m}([L]-[G])\left\{\frac{\tau_n^m}{2}\right\} \tag{41}$$

Due to its reasonable fidelity and computational efficiency, majority of the commercial tools adopts this model for flight mechanics and aero elasticity analyses of rotorcrafts. Therefore, it is quite useful for real time applications and transient analyses. In terms of ground effect, original dynamic wake model contains empirical relations in order to be used in full ground effect case. However, only uniform components of the induced velocity, which are constant everywhere on the rotor disk, are affected due to the presence of the ground. With the inclusion of finite-state ground effect model, not only full but also inclined ground effect case can be simulated in both hover and forward flight. Pressure perturbation on ground plane in rotor wake is represented as an additional pressure perturbation. Finally, the induced velocity at rotor disk in ground effect is calculated based on superposed pressure perturbations of the rotor and the ground. The derivation of the finite-state ground effect model is given in Ref. [6] and correlations with empirical relations, wind-tunnel test data and model rotor test data are reported in Ref. [12]. In order to integrate the finite-state ground effect model to TOROS, the matrix G in (41) (ground influence coefficient matrix) is obtained. Later, it is superposed with gain matrix $[L]$ to include non-uniform ground effects to the trim. Results shown in this study are based on the same expansion for the main rotor inflow and ground effect models. For example, 1x1 Peters-He inflow model together with ground inflow matrix, which is expanded up to its third harmonics. Therefore, both gain matrix $[L]$ and ground influence $[G]$ are three by three square matrices.

Prior to this study, validation of the finite-state ground effect model is made for both full and inclined cases by comparing the ground influence coefficient matrices (G) in Ref. [6]. The G matrix contains r, m harmonics, $j^{th}$ and $n^{th}$ radial mode shape together with associated cosine and sine parts $\left(G_{jn}^{rm}\right)^{cs}$. The indexing of G can be found in (42). The validation results for full and inclined ground effect cases at different heights as well as different heading angles are summarized in Table 1. Comparison of these values show that deviations with respect to Ref. [6] may be due to the numerical errors and different integration schemes to generate G matrix in radial, azimuthal coordinates as well as the coordinate along free-stream line. However, results show good agreement with the results given in Ref. [6] and model is internally consistent. All these verification results show that results of the present study are considered accurate for both full and inclined ground effect cases.

$$\begin{bmatrix} (G_{11}^{00})^{cc} & (G_{13}^{00})^{cc} & (G_{12}^{01})^{cc} & (G_{14}^{01})^{cc} & (G_{12}^{01})^{cs} & (G_{14}^{01})^{cs} \\ (G_{31}^{00})^{cc} & (G_{33}^{00})^{cc} & (G_{32}^{01})^{cc} & (G_{34}^{01})^{cc} & (G_{32}^{01})^{cs} & (G_{34}^{01})^{cs} \\ (G_{21}^{10})^{cc} & (G_{23}^{10})^{cc} & (G_{22}^{11})^{cc} & (G_{24}^{11})^{cc} & (G_{22}^{11})^{cs} & (G_{24}^{11})^{cs} \\ (G_{41}^{10})^{cc} & (G_{43}^{10})^{cc} & (G_{42}^{11})^{cc} & (G_{44}^{11})^{cc} & (G_{42}^{11})^{cs} & (G_{44}^{11})^{cs} \\ (G_{21}^{10})^{sc} & (G_{23}^{10})^{sc} & (G_{22}^{11})^{sc} & (G_{24}^{11})^{sc} & (G_{22}^{11})^{ss} & (G_{24}^{11})^{ss} \\ (G_{41}^{10})^{sc} & (G_{43}^{10})^{sc} & (G_{42}^{11})^{sc} & (G_{44}^{11})^{sc} & (G_{42}^{11})^{ss} & (G_{44}^{11})^{ss} \end{bmatrix} \tag{42}$$

**Table 1: Finite state ground effect model validation with respect to Ref. [6]**

| h (r/R) | δ (deg) | ψ (deg) | **Ref.** [6] | **Present Study** |
|---|---|---|---|---|
| 0.5 | 0 | 0 | $\begin{bmatrix} +0.277073 & +0.039207 & 0.000000 & 0.000000 & 0.000000 & 0.000000 \\ -0.066288 & +0.008585 & 0.000000 & 0.000000 & 0.000000 & 0.000000 \\ 0.000000 & 0.000000 & +0.075118 & +0.017687 & 0.000000 & 0.000000 \\ 0.000000 & 0.000000 & -0.013539 & +0.001178 & 0.000000 & 0.000000 \\ 0.000000 & 0.000000 & 0.000000 & 0.000000 & +0.075118 & +0.017687 \\ 0.000000 & 0.000000 & 0.000000 & 0.000000 & -0.013539 & +0.001178 \end{bmatrix}$ | $\begin{bmatrix} +0.277017 & +0.039198 & 0.000000 & 0.000000 & 0.000000 & 0.000000 \\ -0.066219 & +0.008681 & 0.000000 & 0.000000 & 0.000000 & 0.000000 \\ 0.000000 & 0.000000 & +0.075192 & +0.017718 & 0.000000 & 0.000000 \\ 0.000000 & 0.000000 & -0.013503 & +0.001228 & 0.000000 & 0.000000 \\ 0.000000 & 0.000000 & 0.000000 & 0.000000 & +0.075192 & +0.017718 \\ 0.000000 & 0.000000 & 0.000000 & 0.000000 & -0.013503 & +0.001228 \end{bmatrix}$ |
| 1.0 | 0 | 0 | $\begin{bmatrix} +0.106646 & +0.011428 & 0.000000 & 0.000000 & 0.000000 & 0.000000 \\ -0.033415 & -0.002823 & 0.000000 & 0.000000 & 0.000000 & 0.000000 \\ 0.000000 & 0.000000 & +0.009766 & +0.001677 & 0.000000 & 0.000000 \\ 0.000000 & 0.000000 & -0.002703 & -0.000404 & 0.000000 & 0.000000 \\ 0.000000 & 0.000000 & 0.000000 & 0.000000 & +0.009766 & +0.001677 \\ 0.000000 & 0.000000 & 0.000000 & 0.000000 & -0.002703 & -0.000404 \end{bmatrix}$ | $\begin{bmatrix} +0.106608 & +0.011425 & 0.000000 & 0.000000 & 0.000000 & 0.000000 \\ -0.033398 & -0.002819 & 0.000000 & 0.000000 & 0.000000 & 0.000000 \\ 0.000000 & 0.000000 & +0.009770 & +0.001678 & 0.000000 & 0.000000 \\ 0.000000 & 0.000000 & -0.002702 & -0.000404 & 0.000000 & 0.000000 \\ 0.000000 & 0.000000 & 0.000000 & 0.000000 & +0.009770 & +0.001678 \\ 0.000000 & 0.000000 & 0.000000 & 0.000000 & -0.002702 & -0.000404 \end{bmatrix}$ |
| 1.5 | 0 | 0 | $\begin{bmatrix} +0.049551 & +0.003901 & 0.000000 & 0.000000 & 0.000000 & 0.000000 \\ -0.016890 & -0.001277 & 0.000000 & 0.000000 & 0.000000 & 0.000000 \\ 0.000000 & 0.000000 & +0.001790 & +0.000220 & 0.000000 & 0.000000 \\ 0.000000 & 0.000000 & -0.000578 & -0.000069 & 0.000000 & 0.000000 \\ 0.000000 & 0.000000 & 0.000000 & 0.000000 & +0.001790 & +0.000220 \\ 0.000000 & 0.000000 & 0.000000 & 0.000000 & -0.000578 & -0.000069 \end{bmatrix}$ | $\begin{bmatrix} +0.049526 & +0.003899 & 0.000000 & 0.000000 & 0.000000 & 0.000000 \\ -0.016880 & -0.001276 & 0.000000 & 0.000000 & 0.000000 & 0.000000 \\ 0.000000 & 0.000000 & +0.001791 & +0.000220 & 0.000000 & 0.000000 \\ 0.000000 & 0.000000 & -0.000578 & -0.000069 & 0.000000 & 0.000000 \\ 0.000000 & 0.000000 & 0.000000 & 0.000000 & +0.001791 & +0.000220 \\ 0.000000 & 0.000000 & 0.000000 & 0.000000 & -0.000578 & -0.000069 \end{bmatrix}$ |
| 1.0 | 20 | 0 | $\begin{bmatrix} +0.117026 & +0.011669 & -0.015586 & -0.003052 & 0.000000 & 0.000000 \\ -0.036380 & -0.002617 & +0.005076 & +0.000825 & 0.000000 & 0.000000 \\ -0.014214 & +0.000305 & +0.012746 & +0.002146 & 0.000000 & 0.000000 \\ +0.003331 & -0.000333 & -0.003398 & -0.000468 & 0.000000 & 0.000000 \\ 0.000000 & 0.000000 & 0.000000 & 0.000000 & +0.010850 & +0.001868 \\ 0.000000 & 0.000000 & 0.000000 & 0.000000 & -0.002970 & -0.000441 \end{bmatrix}$ | $\begin{bmatrix} +0.114259 & +0.0120332 & -0.011275 & -0.002357 & 0.000000 & 0.000000 \\ -0.037542 & -0.0030800 & +0.004959 & +0.000912 & 0.000000 & 0.000000 \\ -0.026301 & -0.0022777 & +0.013067 & +0.002436 & 0.000000 & 0.000000 \\ +0.007865 & +0.0002859 & -0.004223 & -0.000695 & 0.000000 & 0.000000 \\ 0.000000 & 0.000000 & 0.000000 & 0.000000 & +0.010683 & +0.001853 \\ 0.000000 & 0.000000 & 0.000000 & 0.000000 & -0.003163 & -0.000498 \end{bmatrix}$ |
| 1.0 | 40 | 0 | $\begin{bmatrix} +0.157563 & +0.013982 & -0.043168 & -0.011356 & 0.000000 & 0.000000 \\ -0.047185 & -0.002180 & +0.013658 & +0.003053 & 0.000000 & 0.000000 \\ -0.039235 & +0.001615 & +0.025861 & +0.005568 & 0.000000 & 0.000000 \\ +0.007083 & -0.001048 & -0.005440 & -0.000887 & 0.000000 & 0.000000 \\ 0.000000 & 0.000000 & 0.000000 & 0.000000 & +0.014993 & +0.002750 \\ 0.000000 & 0.000000 & 0.000000 & 0.000000 & -0.003899 & -0.000609 \end{bmatrix}$ | $\begin{bmatrix} +0.140964 & +0.01613 & -0.02769 & -0.00816 & 0.000000 & 0.000000 \\ -0.053638 & -0.00464 & +0.01413 & +0.00382 & 0.000000 & 0.000000 \\ -0.068269 & -0.00791 & +0.02624 & +0.00744 & 0.000000 & 0.000000 \\ +0.024868 & +0.00143 & -0.01129 & -0.00287 & 0.000000 & 0.000000 \\ 0.000000 & 0.000000 & 0.000000 & 0.000000 & +0.014827 & +0.002898 \\ 0.000000 & 0.000000 & 0.000000 & 0.000000 & -0.004897 & -0.000871 \end{bmatrix}$ |
| 1.0 | 20 | 45 | $\begin{bmatrix} +0.117026 & +0.011669 & -0.011021 & -0.002158 & -0.011021 & -0.002158 \\ -0.036380 & -0.002617 & +0.003589 & +0.000583 & +0.003589 & +0.000583 \\ -0.010051 & +0.000216 & +0.011798 & +0.002007 & +0.000948 & +0.000139 \\ +0.002355 & -0.000236 & -0.003184 & -0.000454 & -0.000214 & -0.000014 \\ -0.010051 & +0.000216 & +0.000948 & +0.000139 & +0.011798 & +0.002007 \\ +0.002355 & -0.000236 & -0.000214 & -0.000014 & -0.003184 & -0.000454 \end{bmatrix}$ | $\begin{bmatrix} +0.114258 & +0.012029 & -0.007973 & -0.001665 & -0.007973 & -0.001665 \\ -0.037542 & -0.003081 & +0.003506 & +0.000645 & +0.003506 & +0.000645 \\ -0.018597 & -0.001609 & +0.011875 & +0.002144 & +0.001192 & +0.000291 \\ +0.005561 & +0.000201 & -0.003693 & -0.000596 & -0.000529 & -0.000098 \\ -0.018597 & -0.001609 & +0.001192 & +0.000291 & +0.011875 & +0.002144 \\ +0.005561 & +0.000201 & -0.000529 & -0.000098 & -0.003693 & -0.000596 \end{bmatrix}$ |
| 1.0 | 20 | 90 | $\begin{bmatrix} +0.117026 & +0.011669 & 0.000000 & 0.000000 & -0.015586 & -0.003052 \\ -0.036380 & -0.002617 & 0.000000 & 0.000000 & +0.005076 & +0.000825 \\ 0.000000 & 0.000000 & +0.010850 & +0.001868 & 0.000000 & 0.000000 \\ 0.000000 & 0.000000 & -0.002970 & -0.000441 & 0.000000 & 0.000000 \\ -0.014214 & +0.000305 & 0.000000 & 0.000000 & +0.012746 & +0.002146 \\ +0.003331 & -0.000333 & 0.000000 & 0.000000 & -0.003398 & -0.000468 \end{bmatrix}$ | $\begin{bmatrix} +0.114259 & +0.012033 & 0.000000 & 0.000000 & -0.011275 & -0.002357 \\ -0.037542 & -0.003080 & 0.000000 & 0.000000 & +0.004959 & +0.000912 \\ 0.000000 & 0.000000 & +0.010683 & +0.001853 & 0.000000 & 0.000000 \\ 0.000000 & 0.000000 & -0.003163 & -0.000498 & 0.000000 & 0.000000 \\ -0.026301 & -0.002278 & 0.000000 & 0.000000 & +0.013067 & +0.002436 \\ +0.007865 & +0.000286 & 0.000000 & 0.000000 & -0.004223 & -0.000695 \end{bmatrix}$ |

## 6 RESULTS

As described in section 2, by adding rolling degree of freedom to the tire, spin-up loads during run on landings can be calculated.

In order to find landing gear loads that are generated during landing with a forward speed, drop test simulations are performed by using TOROS and landing gear model that is generated in commercially available software ADAMS® (see Figure 5). Notice that, in simulations, wheel of the main landing gear is initially rotated at 120 rad/s (which corresponds to 50 knots forward speed) and a drop test is performed. It can be seen that, after tire is in contact with the ground, its rotational speed and slip velocity starts to decrease. Due to friction forces between tire contact patch and ground these parameters vanish very rapidly. It is also shown in Figure 5 that, strut deflections, ground reaction and spring-back forces are similar in both simulations. Therefore, generic ground dynamics model given in this paper is a good candidate for estimating impact loads during landing.

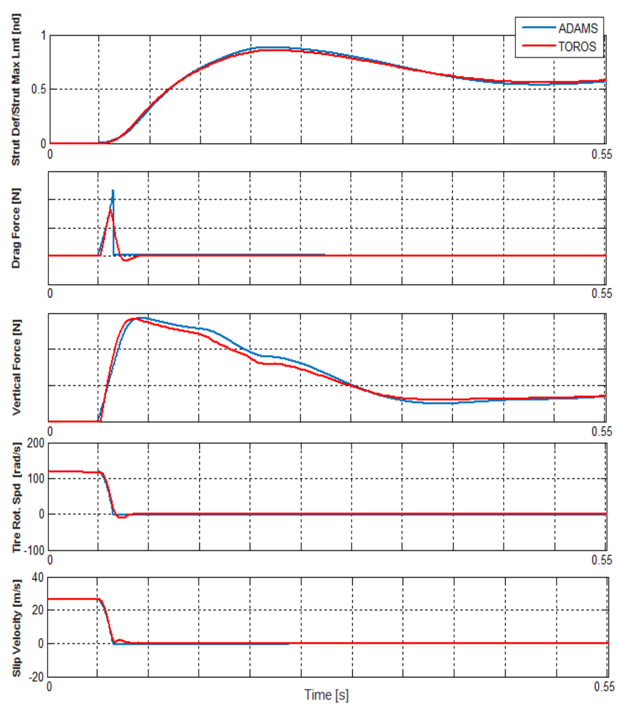


**Figure 5 Drop Test Simulation of Main Landing Gear with an Initial Speed of 50 knots**

In Figure 6, run-on landing simulation results of a helicopter with tricycle landing gear configuration (one nose and two main landing gears) is provided. Helicopter is initially trimmed in ground effect with 20 knots ground speed and by reducing collective at a constant rate, landing gears touch the ground after 3 seconds from the start.

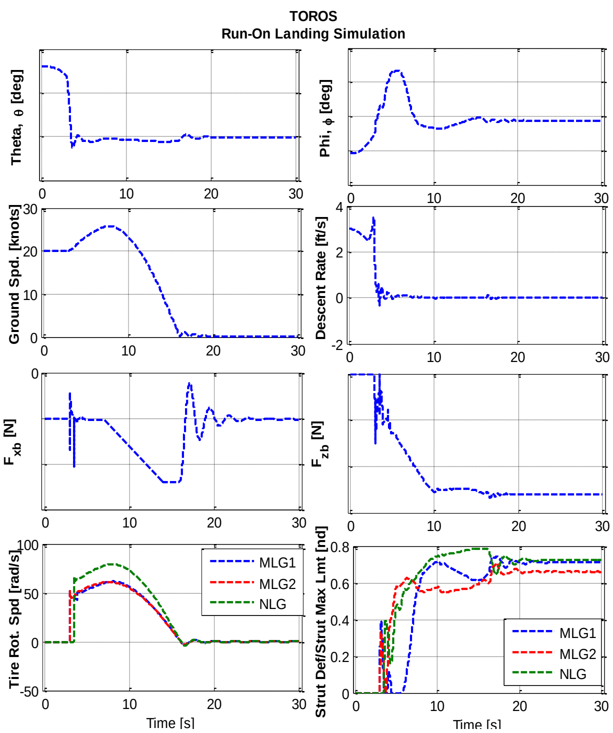


**Figure 6 Run-on Landing Simulation**

Sink rate during touchdown is 3.5 ft/s. Notice that, rotational speed of tires rapidly increase and reach 20 knots after touchdown. After t = 7 [s], brakes are applied and helicopter starts to decelerate. Between t = 14 [s] and t = 16 [s], maximum amount of friction is applied to the helicopter (see $F_{xb}$) and after this point helicopter is stopped.

In Figure 7 and Figure 8 comparison of the trim results are shown for full and inclined ground effect cases. Full ground effect comparison is made with respect to rotor height and results are plotted in Figure 7. Notice that horizontal axis is the helicopter cg height above ground level. Figure 8 illustrates inclined ground effect trim results of a -10$^0$ side-slope (left MLG uphill orientation) landing. Starting from zero roll attitude, helicopter is trimmed with different roll attitudes up to 10 degrees while uphill landing gear is in contact with the ground. Friction forces and moments are included in the results and it is assumed that there is no wind in the environment. In both figures, control inputs, roll attitudes, conning, longitudinal and lateral flapping angles, total power differences of main and tail rotor with respect to uniform GE case together with non-dimensional first harmonics of uniform, longitudinal and lateral induced velocities are shown. Flapping sign convention for positive angles can be summarized as cone up for $\beta_0$, rotor disk forward tilt for $\beta_{1c}$ and left tilt for $\beta_{1s}$ when viewed from aft of the helicopter. Results are obtained with 1x1 (3-states)

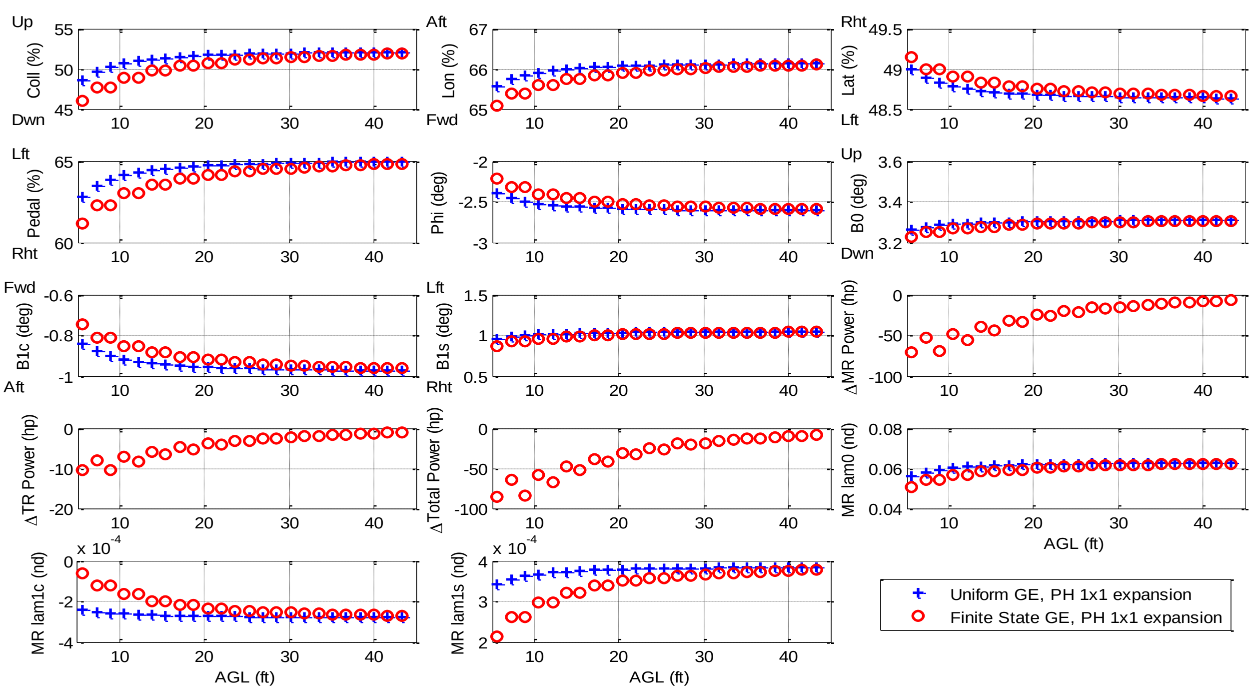


**Figure 7 Comparison of Trim Results in Full Ground Effect**

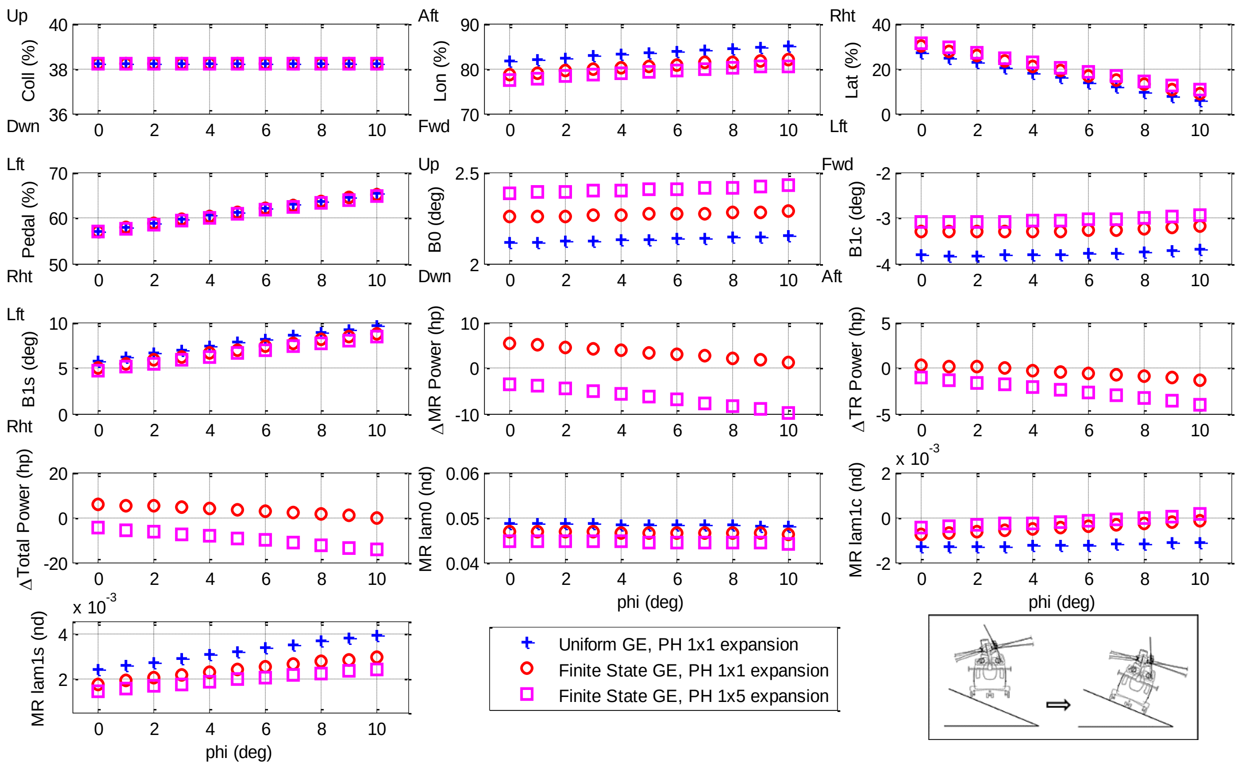


**Figure 8 Comparison of Trim Results in Inclined Ground Effect during Left LG Uphill Slope Landing**

Peters-He inflow model (PH, 1x1). In addition, for the slope landing trims (i.e. inclined ground case), radial mode shape is expanded to 1x5 (9-states) in order to examine the radial inflow and ground effect influence on the trim results.

For the initial studies, each blade is divided to 10 segments based on equal annulus approach to calculate blade aerodynamic loads in blade element theory. In addition, these results show that finite state ground effect model changes the results for both full and inclined ground effect cases. In both ground conditions, inflow distribution on the rotor disk changes with respect to uniform ground effect model. For full ground effect case, as rotor height decreases, finite state ground effect model results in higher ground effect intensity yielding less power demand. For inclined ground case, significant margin gain in lateral cyclic (~5%) is observed among uniform and finite state ground effect models. Higher order inflow model (PH 1x5) associated with higher order ground influence with finite state ground effect model has a small effect on trim results compared to PH 1x1 expansion. However, further investigation was also conducted to quantify the effect of higher order inflow and ground effect models. For these results, radial expansion is made up to fifth harmonics and azimuthal expansion is also examined up to second harmonics. The combinations and total number of inflow states are given in Table 2. Since radial inflow state number is expanded up to $5^{th}$ harmonics, radial segment number is increased to 30 to be consistent with higher order radial expansion in inflow selection. Inflow state selection results are summarized in Table 2.

**Table 2: Inflow State Selection and Total Inflow States**

| Highest radial harmonics, r | Highest azimuthal harmonics, m | Total Inflow States |
|---|---|---|
| 1 | 1 | 3 |
| 2 | 1 | 4 |
| 3 | 1 | 6 |
| 4 | 1 | 7 |
| 5 | 1 | 9 |
| 2 | 2 | 6 |
| 3 | 2 | 8 |
| 4 | 2 | 11 |
| 5 | 2 | 13 |

Trim results are given in Figure 9, Figure 10, Figure 11 and Figure 12. On those figures, horizontal axis is roll angle $\phi$ and uniform ground effect case is shown with dashed and non-uniform finite state ground effect model is shown with solid lines. All of the power differences are plotted with respect to the associated uniform ground effect model results. Considering the trim results given in Figure 9 and Figure 10, all of the cases yield different trim results with respect to associated uniform ground effect cases. In other words, longitudinal and lateral cyclic positions deviates approximately 3% and 4%, respectively.

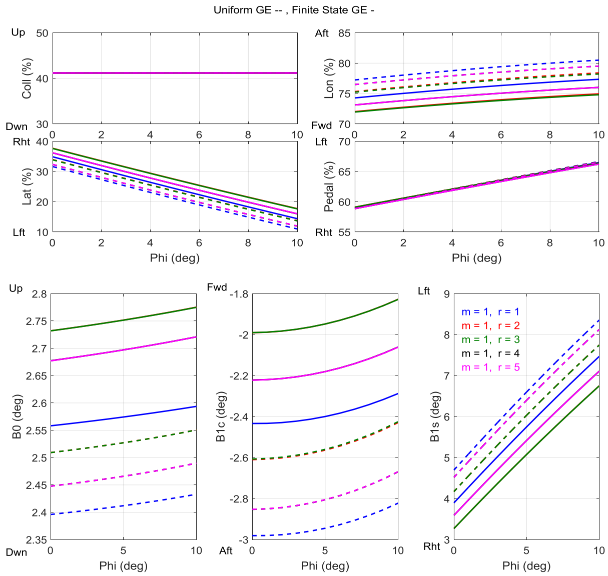


**Figure 9: Comparison of Trim Results (Controls and MR Flapping Angles) for Different Radial Harmonic Numbers**

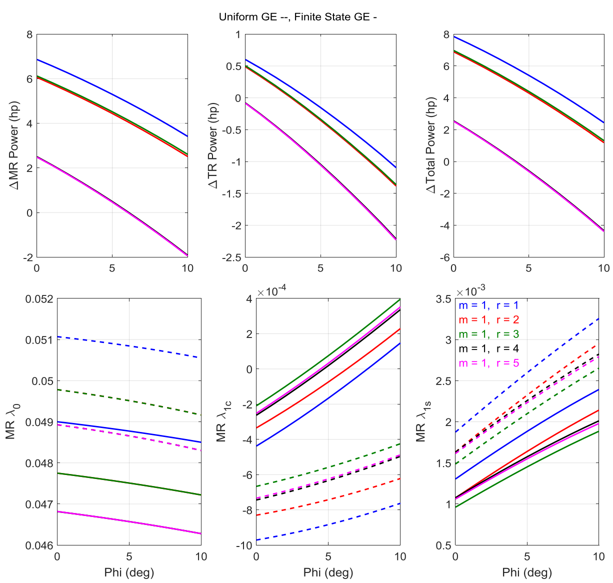


**Figure 10 Comparison of Trim Results (Power Differences with Respect to Uniform GE Model and MR Inflow States) for Different Radial Harmonic Numbers**

It can be concluded that different tip path plane orientations are valid considering the flapping angles of the main rotor. For both uniform and non-uniform ground effect cases, trim results for PH 1x2 and 1x3 are very similar to each other. A similar behavior is also seen between PH 1x4 and 1x5. The negligible difference can be seen in main rotor inflow states. Increasing the radial harmonic number results in lesser power differences. However, differences are negligible (Maximum 8 hp difference in total power). Increasing the harmonic number to 2 from 1 in azimuthal direction yields no difference. In other words, results for PH 1x2 and 2x2, 1x3 and 2x3, 1x4 and 2x4, 1x5 and 2x5 are identical. Therefore, only PH 1x3 and 2x3, 1x5 and 2x5 are shown in Figure 11 and Figure 12. In addition to the trim results, aerodynamic parameters such as angle of attack (AOA) and lift generated by main rotor were also examined.

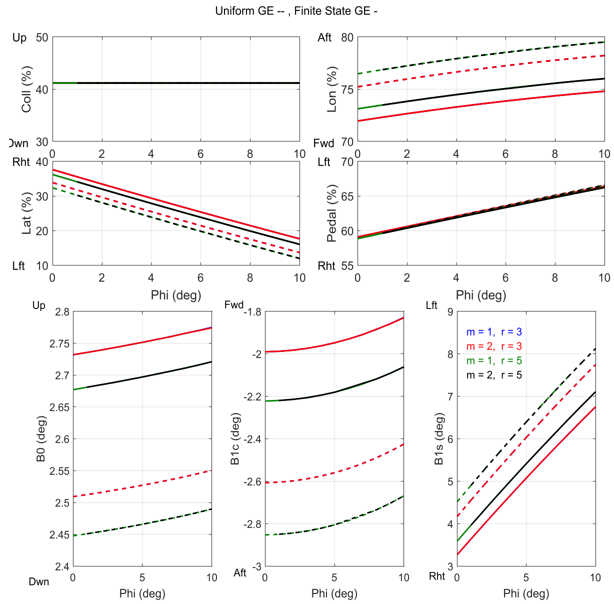


**Figure 11 Comparison of Trim Results (Controls and MR Flapping Angles) for Different Radial Harmonic Numbers**

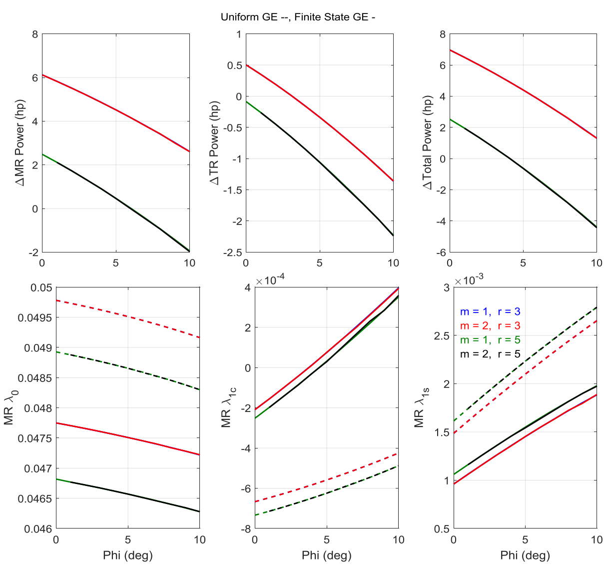


**Figure 12: Comparison of Trim Results (Power Differences with Respect to Uniform GE Model and MR Inflow States) for Different Radial Harmonic Numbers**

In Figure 13, Figure 14, Figure 15 and Figure 16, AOA and lift contour plots of main rotor are given for three different roll angle instances ($\phi = 0, 5, 10$ degrees).

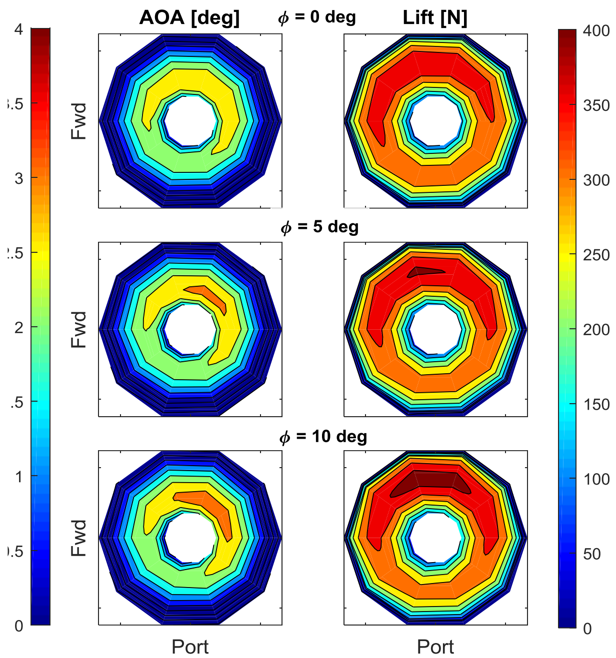


**Figure 13: Uniform GE, m = 1, r = 1**

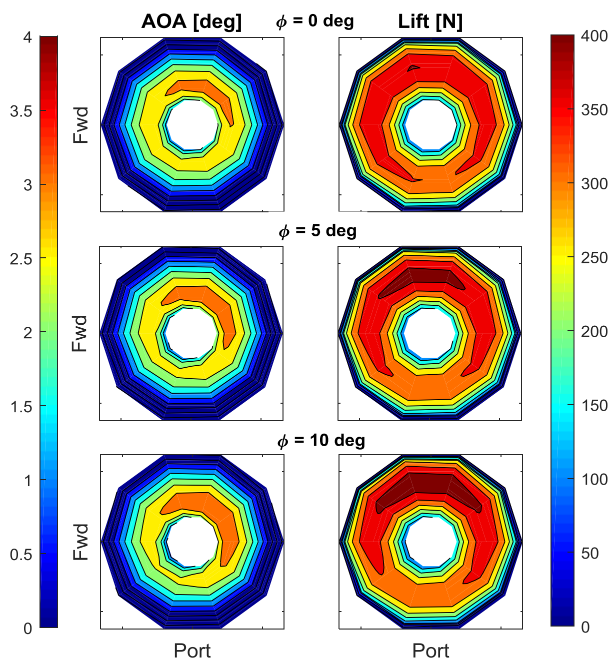


**Figure 14: Finite state GE, m = 1, r = 1**

In Figure 13 and Figure 15, uniform GE contour plots are given for PH 1x1 and 1x5 whereas Figure 14 and Figure 16 show finite state counterparts. For consistency, these contour plots are scaled so that maximum AOA is 4 degrees and maximum lift force is 400 N. It was previously mentioned that finite state GE model shows higher ground effect intensity. Contour plots verify this since AOA and lift increase is evident on the starboard side. In other words, rotor efficiency increases with respect to uniform GE model for all cases. Therefore, these contour plots are only given for PH 1x1 and 1x5 for brevity.

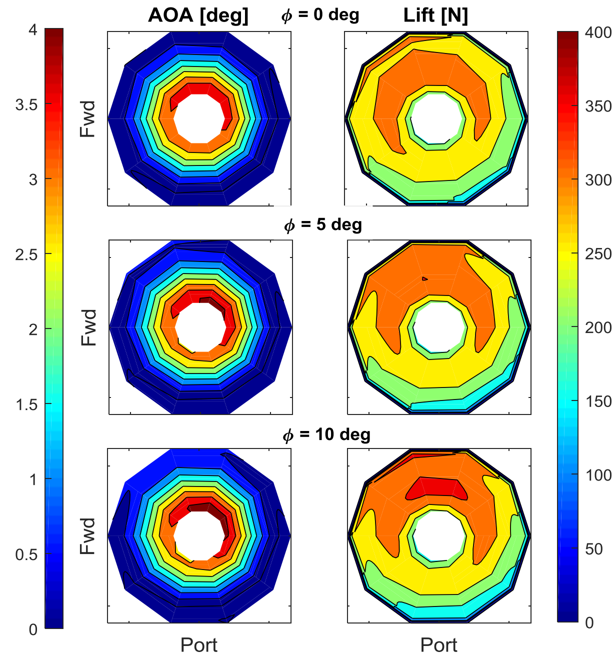


**Figure 15: Uniform GE, m = 1, r = 5**

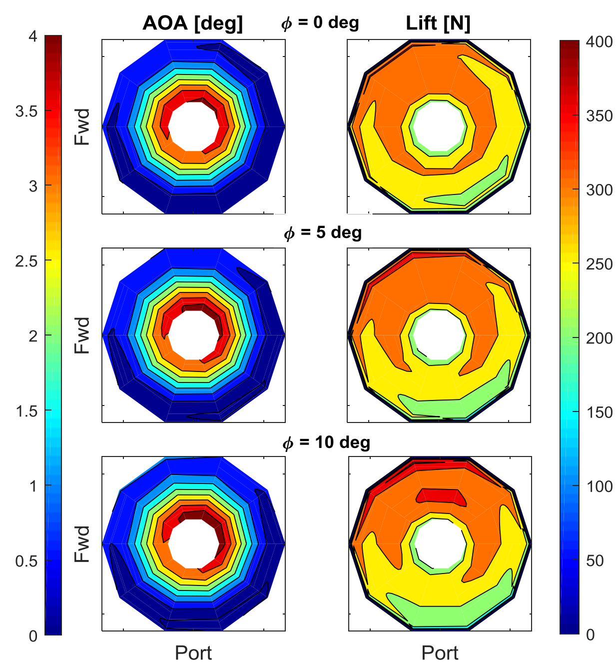


**Figure 16 Finite state GE, m = 1, r = 5**

Comparing the PH 1x1 and 1x5 case among finite state GE cases, PH 1x1 case results in higher roll moments towards upslope resulting in higher $\beta_{1s}$ values considering Figure 9 together with lift contours. Therefore, PH 1x1 case results in lesser margin (~1.3%) for the left limit of the lateral cyclic stick. However, maximum difference for lateral cyclic occurs between PH 1x1 and PH 1x3 cases given by blue and green solid lines in Figure 9. This time 3.25% lesser margin is seen for left limit of the lateral cyclic stick.

Figure 17 shows inclined ground effect results when helicopter is trimmed at different pitch attitudes along -5$^0$ down-slope (left and right MLGs uphill orientation). Contour plots of two different pitch attitudes (0 and -5 degrees) are given for illustration.

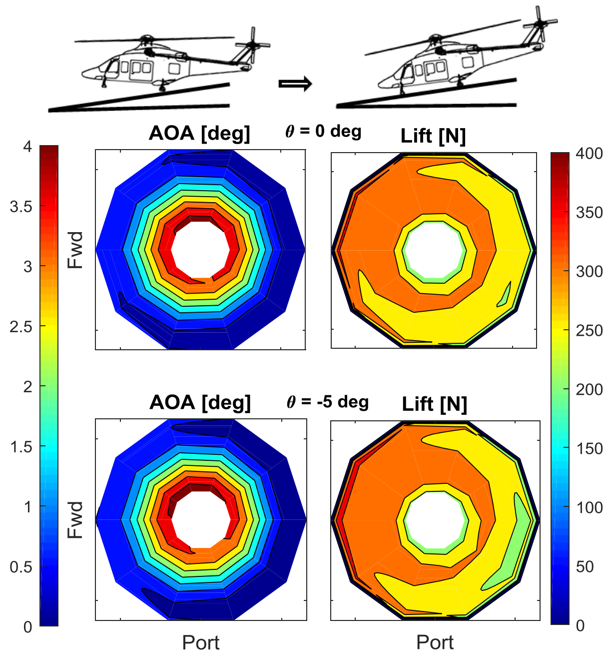


**Figure 17 Finite state GE, m = 1, r = 5**

Results are similar to the side-slope landing case, where ground effect intensity increases on the downhill side resulting in increased lift force on the forward side of the main rotor disc. When contour plots given in first two rows of Figure 16 and Figure 17 are compared, it can be seen that approximately 90 degrees of phase shift exists since helicopter is trimmed along the slope instead of across the slope.

## 7 CONCLUSIONS

By coupling a generic ground dynamics model with a high fidelity helicopter model accurate estimations of helicopter behavior on ground can be made before conducting any flight test. It is possible to determine required control ranges on ground, to check whether the aircraft is controllable or not during (slope) landing and take-off, taxi, rolling take-off, run-on landing and also to estimate impact loads during touchdown.

In order to understand the effect of non-uniform inflow parameters on slope landing maneuver, high fidelity finite state ground effect model [6], which is capable of modelling inclined ground effect, was used. Results showed that, finite state ground effect model affected the control margins and main rotor flapping especially during slope landing and take-off analyses. The principal findings are as follows:

- Finite state GE model shows higher ground effect intensity with respect to uniform GE model yielding to higher lift generated by the main rotor on the upslope side.
- From flight mechanics aspect, cyclic stick positions may deviate up to 4% with the inclusion of finite state ground effect model.
- The combined effect of state selection for main rotor inflow and ground effect models has a complex nature and affects the trim results for power, tip path plane orientation and cyclic stick positions, which need to be considered thoroughly in future studies.

## ACKNOWLEDGMENTS


The authors would like to acknowledge Mr. Fatih Çetin from landing gear design group and Mr. Anıl Öztürk from simulation software group for their valuable contributions to the study.


## REFERENCES


[1] J. Daniels, "A Method for Landing Gear Modeling and Simulation with Experimental Validation," NASA Contractor Report 201601, NASA Langley Research Center, Hampton, Virginia, 1996.

[2] J. McGehee and H. Carden, "A Mathematical Model of an Active Control Landing Gear for Load Control During Impact And Roll-Out," NASA Technical Note TN D-8080, NASA Langley Research Center, Hampton, Virginia, 1976.

[3] H. Passmore and C. Korba, "DC-9 Landing Gear Math Model for Directional Control on Runway Flight Simulation," McDonnell Aircraft Company Report MDC A4816, McDonnell Aircraft Company, Saint Louis, Missouri, May 1977.

[4] J. Howlett, "UH-60A Black Hawk Engineering Simulation Program: Volume I – Mathematical Model," NASA Contractor Report 166309, December 1981.

[5] Anon., "Aeronautical Design Standard, Performance Specification, Handling Qualities

Requirements for Military Rotorcraft," USAAMCOM, ADS-33E-PRF, 21 March 2000.

[6] H. Xin, "Development and Validation of a Generalized Ground Effect Model for Lifting Rotors, Ph.D. Thesis," Georgia Institute of Technology, July 1999.

[7] N. Iboshi, T. Nagashima and J. Prasad, "Experimental Validation of an Inclined Ground Effect Model," American Helicopter Society, Washington DC, 2001.

[8] K. Sansal, V. Kargın and U. Zengin, "A Generic Ground Dynamics Model for Slope Landing Analysis," in *72nd Annual Forum of the American Helicopter Society*, West Palm Beach, Florida, May 17-19, 2016.

[9] K. Şansal, G. Koçak and V. Kargın, "Multi-objective Horizontal Stabilizer Optimization Using Genetic Algorithm," in *AHS International 74th Annual Forum & Technology Display*, Phoenix, Arizona, May 14-17, 2018.

[10] P. Evans, M. G. Perhinschi and S. Mullins, "Modeling and Simulation of a Tricycle Landing Gear at Normal and Abnormal Conditions," in *AIAA Modeling and Simulation Technologies Conference*, Toronto, Ontario Canada, 5 August 2010.

[11] C. J. He, "Development and Application of a Generalized Dynamic Wake Theory for Lifting Rotors, Ph.D. Thesis," Georgia Institute of Technology, July 1989.

[12] H. Xin, J. Prasad, D. A. Peters, N. Iboshi and T. Nagashima, "Correlation of Experimental Measurements with a Finite-State Ground Effect Model," American Helicopter Society, Virginia Beach, May 2000.